Robotica (2005) volume 23, pp. 501–513. © 2005 Cambridge University Press
doi:10.1017/S0263574704001171 Printed in the United Kingdom

A novel ultra-precision integrated robotic system

ShaoWei Gong

Green Standard Technologies, 881 Spring Valley Drive, Cookeville, TN 38501 (USA)
E-mail: shaoweig@hotmail.com

(Received in Final Form: October 13, 2004)

SUMMARY
An ultra-precision integrated robotic system is developed, which integrates a passive robotic measurement system (shadow system) with an industrial robot. The shadow system is built almost ideal. In a working process, when the end-effecter of integrated robot is driven to a target with errors which are caused by degrading factors associated with the robot, the shadow system will independently detect the end-effecter frame instantly with ultra-precision kinematic accuracy. A scheme of approach control is then established to drive the end-effecter of the integrated robot to compensate the error step by step until the desired target is achieved with ultra-precision positioning accuracy.

KEYWORDS: Ultra-precision; 6-D robot; Shadow system; RYLDA; Kinematic accuracy.

I. INTRODUCTION

An industrial robot possesses its very unique and advanced properties. If there were no influences of degrading factors existing with a robot to drag down its kinematic accuracy, it would be one of the most important items of equipment in automation of ultra-precision engineering. Here, kinematic accuracy refers to both the position and orientation accuracies of end-effecter frame of a robot. Generally speaking, the following damaging influences caused by some degrading factors are considered the major problems to block its possible key role in ultra-precision engineering:

- The influence of manufacturing and assembling tolerance and clearance
- The influence of varying deflection under different payloads and geometric change of the linkage
- The influence of correlation between uncertain non-linear deflection and system configuration
- The influence of kinematic clearance and the wear of kinematic pair
- The influence of associated problems with the gap of kinematic clearance and wear
- The influence of ambient conditions, especially, the temperature, etc.

If these above problems can be resolved, it will be easy for a robot to achieve ultra-precision kinematic accuracy. However, the difficulty is that these degrading factors are inevitable since they are associated with the nature of design, manufacturing, assembly, and application of a robot. As a result, to date, the kinematic accuracy of an industrial robot is still relatively low. For example, in the development of a precision robotic computed tomography (CT) inspection system with Green Standard Technologies, a 6 degree-of-freedom (DOF) rigid body robot with the kinematic accuracy in level of {0.025 mm, 5 arc-second} yielding different payloads is urgently sought; however, on today's robotic market, such a precise robot is still not available.[1]

Obviously, if a robot yielding rigid body guidance is unable to achieve precision kinematic accuracy, a robot yielding large deflection analysis (RYLDA, i.e. the semi-flexible and the flexible robotic systems) is absolutely no chance to play a role in precision engineering. It is known that a RYLDA can have large payload/weight ratio and some attractive dynamic properties. However, with a RYLDA, all the above degrading factors exist; moreover, the problems associated with deflection become extremely serious. The uncertainties of nonlinear correlations of deflection and system configurations make the RYLDA too difficult to be controlled. With investigation, it shows that, by now, no 6 DOF RYLDA has been developed yet in real application with the acceptable kinematic accuracy and the "under-control" manner.[2–7]

It is noted that, in recent years, visual servoing technology of robotics is playing a more and more important role in robotic kinematic control. Undoubtedly, the visual servoing technology possesses its unique technical attractiveness. It appears very promising to bring significant development for a robot to achieve precision kinematic control in the future. However, visual servoing technology used in robotics can still only implement relatively simple applications with rough kinematic accuracy by employing artificial markers to circumvent the end-effecter and kinematic data. Recently, some developments have allowed the servoing systems to deal with real-time control for relative complex applications with no or very limited markers for better tracking accuracy. However, so far, an industrial robot with the application of visual servoing technology is still unable to achieve the precise kinematic accuracy control. It is noted that the linear positioning accuracy of a robot with visual servoing technology varies with different trajectories in working domain, in general, it may only achieve the positioning accuracy roughly around $0.1 \sim 1$ mm level.[8–12]

At current stage, how to achieve the goal to develop an ultra-precision industrial robot still presents a great challenge in robotics. In such a situation, the efforts with this research present a novel and useful design methodology and a workable embodiment to achieve such a goal for the development of ultra-precision industrial robot.

https://doi.org/10.1017/S0263574704001171 Published online by Cambridge University Press

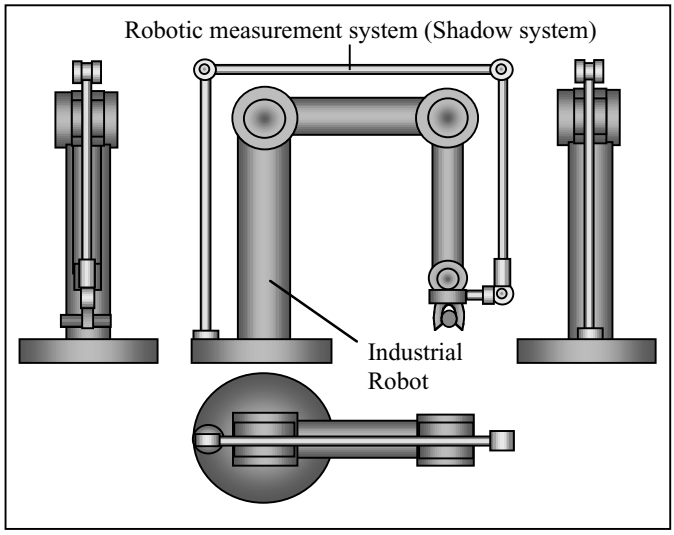


Fig. 1. An Embodiment of Ultra-precision Robotic System.



Fig. 2. An Ultra-precision Robotic CT Inspection System (By curtsey of Green Standard Technologies, Cookeville, TN, USA).

II. DEVELOPMENT OF A NOVEL ULTRA-PRECISION INTEGRATED ROBOTIC SYSTEM

II.1. Shadow system

To deal with the inevitable degrading factors for the development of an ultra-precision industrial robot, an integrated robotic system is proposed, which integrates a passive robotic measurement system (shadow system) with an industrial robot. The shadow system consists of linkages, kinematic joints, and measurement sensors that are mated with the kinematic joints to form a passive servo-measurement system with proper degree-of-freedom to monitor the position of an end-effecter of a robot with its own end-effecter through the connection-point. Figure 1 depicts the basic structure of such a 6-D ultra-precision robotic system, which is formed by a 6-D shadow system and a 6-D industrial robot. The 6-D robot and the 6-D shadow system are connected together through the origin of end-effecter frame. Figure 2 depicts such a robotic system in conjunction with a computed tomogtaogy (CT) inspection system to provide an advanced ultra-precision robotic CT inspecting process for different objects with the same platform.

From Fig. 1 and Fig. 2, it is known that the shadow system has formed a control loop independent of the mated conventional industrial robot to determine the position and orientation of the end-effecter frame. It means that all these degrading factors associated with the mated robot have nothing to do with the control loop formed by the shadow system. In a control process, the control loop of the shadow system can communicate directly with the control system to determine the exact position and orientation of the end-effecter frame.

In robotic kinematic control, it is known that when a robot is needed to send its end-effecter to a desired target, at first, it finds the inverse kinematic solutions and excites its actuators yielding corresponding configurations. If the robot is ideal, then the end-effecter can exactly reach the desired position and orientation of target without error. However, because of the damaging influences of degrading factors, a robot is not able send its end-effecter to the desired target, and cannot even identify the exact position and orientation of its end-effecter frame after the excitation.

In this research, because of the use of the shadow system, the integrated robotic system can detect the differences between the target and its end-effecter frame after the excitation. By using the differences, the control system can then move the end-effecter frame to approach the desired position and orientation of target. Through the scheme of approach control step by step, the robotic system can finally achieve the desired target frame.

With this process of approach control, obviously, the kinematic accuracy of the integrated robotic system only relies on the measurement accuracy of the shadow system. It is noted that the shadow system can be made almost ideal. The following discussions are for the best understanding of why the shadow system can be considered almost ideal with ultra-precision measurement accuracy. It explains why such design method and embodiment can meet the requirements for the development of an ultra-precision integrated robotic system.

II.2. Discussions about the favorable conditions to build an almost ideal shadow system

II.2.1. Shadow system can be considered as an almost ideal weightless rigid body system. The shadow system is a passive system. It is simply pulled by the connection point (CP) on the end-effecter with insignificant resistance. It means any load acting on the industrial robot have nothing to do with the shadow system. Since it stands no load, the shadow system can be made very light. Therefore, there will be only insignificant forces of friction, gravity, and dynamic force acting on the system. Since the linkages of the system can be relatively strong and the weight of the system can also be much lighter than the robot, it means that the deflection and the weight of the shadow system can be ignored. Therefore, the shadow system can be considered as a nearly ideal weightless rigid body system. As a result, in general situation, it conducts

https://doi.org/10.1017/S0263574704001171 Published online by Cambridge University Press

a. The influence of deflection of the component of shadow system is minor and can be ignored
b. The dynamic influence of shadow system to interact with the robot is minor and can be ignored

II.2.2. The influence of tolerance and clearance error can be controlled in nm level. The errors caused by tolerance and clearance are inevitable associated with the nature of manufacturing and assembling of the monitoring system. However, such errors will not degrade the accuracy of the shadow system. It is noted that the dimensions of the system are fixed and unchangeable once the system is assembled. After assembly, the actual dimension of the system can be measured as the real structural nominal parameter to replace the originally designated structural nominal parameter. The error to measure the real nominal parameter is the accuracy of the measurement instrument.

Currently, there are several existing measurement technologies to control the dimensional error of measurement <1 nm. One of such technologies is the Michelson laser interferometer platform.[13,14] It is noted that a conventional Michelson platform may not conduct absolute dimensional measurement. However, a specialized Michelson linear measurement platform can be developed to measure the absolute dimension for the calibration of the length of the parameters of the shadow system. Such a mechanical press measurement or optical observation platform can be built with a series of modules with standard length based on the same method in reference [15]. As to the angular calibration of the shadow system, an angular measurement device can be developed based on the measurement of arc length of a rotating measurement jig with a Michelson laser interferometer platform.

II.2.3. The error of kinematic clearance. The kinematic clearance designed for kinematic pair is to guarantee the relative motion between connected components. After the assembly, there will be uncertain gap for the relative motion between the components. The gap is a major problem to degrade kinematic accuracy, and is also the source for contamination, backlash, and thin film of lubrication. Usually, this problem cannot be avoided. However, if there is no force or only very small force acting on the motion pair, a very light duty ultra-precision bearings with zero clearance can be used to form a revolute joint pair. In such a case, since the rollers can rotate on races with pure rolling of non-gap motion, the error of clearance between the rolling rollers and the races are insignificant and can be ignored. It is noted that the light-duty elastic rubber roller bearings with zero or slightly lapped over clearance may also be used to eliminate the joint gap.

II.2.4. Measured joint rotational displacement error. In the design of shadow system, an ultra-precision rotary optical encoder is mated with ultra-precision bearings mounted at the revolute joint pair. Since the reading of the optical encoder is unique and the optical encoder is directly to measure the relative angular displacement of joint shaft and joint house, the measurement error of rotational displacement yields the resolution of optical rotary encoder.

On the current market, the resolution of an existing common optical rotary encoder with 3.5 in diameter can achieve 4,608,000 counts/revolution reference [1]. If such an optical encoder is used to build the shadow system, the measurement error of rotational displacement is about 0.28 arc-second. The finer the resolution of employed rotary encoder, the less the measurement error of the rotational displacement. It is also noted that if an ultra-precision rotary encoder with 32-bit resolution on the market can be used to build the shadow system, the measurement error of rotational displacement is about 3×10^{-4} arc-second.

II.2.5. Wear between kinematic joints can be ignored. Since there is no load on the shadow system and the frictional forces acting on the joints are insignificant, the wear of the kinematic joints can be ignored for quite a long time period.

II.2.6. Vibration is not a problem with rigid body robot and can be moderated with very flexible case. Although the system with the research can be made relatively light to have the advantage of small weight/payload ratio, it can still be designed quite "rigid". In general, if the integrated industrial robot is based on the design of rigid body guidance, the vibration of the system will not be an obstacle to the development of the ultra-precision robotic system.

For the special case of RYLDA with very flexible robot, to control the vibration of linkages, dampers may be needed since the influence of vibration delays the approaching process. It is noted that there are some existing and developing technologies, such as magnetic damper, PZT actuator, embodied skin gauge and controller, etc., which can be adopted to deal with the problem. Vibration of flexible robot is still an on-going independent research.[16-18] In the future, more proper technologies will be developed to effectively resolve such a problem. Generally speaking, with proper dampers, the vibration of a RYLDA can be settled down fast.

II.2.7. The shadow system can have a good and stable working condition. Since the shadow system is an independent system, it is easy to provide an isolated environment to keep good and stable working conditions to resist the influence of the ambient conditions in work cells. It is known that the ambient conditions in robotic work cells, especially the temperature, may drag down the measurement accuracy of the shadow system. However, to guarantee the success of the research and prevent the system from the influence of ambient conditions, the following four methods basically used in current ultra-precision engineering practices will be considered:

a. Use cooling agent to control the change of temperature caused by heat sources
b. Restrict the working cell of the system in designated working condition
c. Have an isolation design to isolate the system from all heat sources
d. Design an ambient condition control system to cover the equipment

Generally speaking, the temperature influence is not particular with this research, and it is a general problem associated

https://doi.org/10.1017/S0263574704001171 Published online by Cambridge University Press

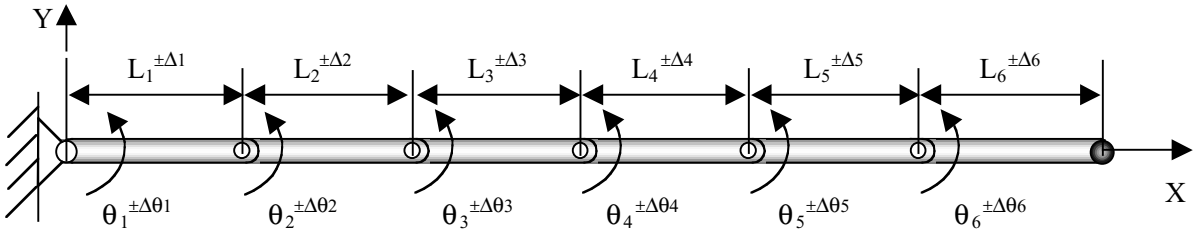


Fig. 3. A case of extremely built 6-D rotational joint robot.

with all ultra-precision kinematic control technologies. To control the change of environment temperature is a basic requirement with the development of micro- or nano-technology. With all or partial of the above conventional methods, it appears that there is no difficulty to control temperature errors in the designated ambient conditions in precision engineering practice to achieve ultra-precision measurement accuracy. It is noted that with a robot the influence of temperature is relatively less important since there is usually no significant heat sources involved.

II.2.8. Rough estimation of the measurement accuracy of the shadow system. The measurement accuracy of a shadow system can be roughly estimated with study of an extreme case. If a 6-D robotic system with 6 dimensional linkages is adopted to build the passive shadow system, the measured maximum linear error will not be larger than

$$\Delta D_X = \pm \sum_{i=1}^{6} |\Delta_i| \tag{1}$$

with the extreme design of a 6-joint robot shown in Fig. 3. Here, ΔD_X is the linear dimensional error in X direction, and Δ_i is the measurement error to measure element i. As is mentioned above, Δ_i can be controlled in 1 nm level with a specialized Michelson interferometer measurement platform. The total error in X direction is 6 nm. With reference of Fig. 3, it is known that the linear dimensional error in Y direction is caused by rotational error, and the maximum linear dimensional error is

$$\Delta D_Y = L_1 \cos \Delta\theta_1 + L_2 \cos(\Delta\theta_1 + \Delta\theta_2) + \cdots + L_6 \cos(\Delta\theta_1 + \cdots + \Delta\theta_6) < \sum_{i=1}^{6} |L_i \, \Delta\theta_i| \tag{2}$$

Here, assume that each of the links of the robot is 500 mm. It is noted that, if the common rotary encoder with 0.28 arc-second resolution is used with the development, the maximum linear dimensional error caused by the rotational error in Y direction is about 4 μm. If the 32-bit ultra-precision rotary encoder with 3×10^{-4} arc-second resolution is used, then the maximum linear dimensional error caused by the rotational error in Y direction can be about 4 nm.

In this research, the ultra-precision rotary encoder with 32-bit resolution is discussed to emphasize that such an ultra-precision robotic system is able to achieve nm positioning accuracy. Also, the common encoder with 0.28 arc-second resolution is considered as an embodiment of design in industrial practice as the low expectations. It is noted that, with the case of using 32-bit resolution encoder, Δ_i should be controlled in 1 nm level to match the overall ultra-precision accuracy. With the case of using 0.28 arc-second resolution encoder, Δ_i can only be controlled in 1 μm level to match the overall error for easing the calibration condition.

Obviously, if the extreme robot in Fig. 3 is adopted as the passive shadow system, the measured maximum rotational error of yaw without the influence of structural correlation will not be in excess of

$$\Delta\theta = \sum_{i=1}^{6} |\Delta\theta_i| \tag{3}$$

around Z axis. Here, $\Delta\theta$ is the rotational displacement measurement error of yaw, and $\Delta\theta_i$ is the measurement error to measure the rotational displacement of joint i. As above-mentioned, $\Delta\theta_i$ yields the resolution of the rotary encoder. The absolute errors of the shadow system with the extreme design of a robot can then be obtained, and

$$\mathrm{ERR}_{\mathrm{Absolute}} = \left\{ \left(\Delta D_X^2 + \Delta D_Y^2 \right)^{1/2}, \Delta\theta \right\} \tag{4}$$

If the 4,608,000 resolution encoder is adopted, it leads to $\mathrm{ERR}_{\mathrm{Absolute}} = \pm\{7.21\ \mu\mathrm{m},\ 1.8\ \text{arc-second}\}$. If the 32-bit resolution encoder can be used, it leads to $\mathrm{ERR}_{\mathrm{Absolute}} = \pm\{7.21\ \mathrm{nm},\ 1.8 \times 10^{-3}\ \text{arc-second}\}$. Since the analysis is based on the extreme case of a 6 DOF robot, with the conservative estimations, the following rounded goals for the development of ultra-precision robotic system are expected:

Low expectation with 4,608,000 resolution encoder:

$$\mathrm{ERR}_{\mathrm{Absolute}} = \{10\ \mu\mathrm{m},\ 2.5\ \text{arc-second}\}$$

High expectation with 32-bit resolution encoder:

$$\mathrm{ERR}_{\mathrm{Absolute}} = \{10\ \mathrm{nm},\ 10^{-2}\ \text{arc-second}\}$$

II.3. Inverse kinematics of the ultra-precision integrated robotic system

With reference of Fig. 1, Fig. 2, and Fig. 4, the inverse kinematics of a 6 DOF ultra-precision integrated robotic system to move its end-effecter frame to a desired target can be determined. In Fig. 4, $\{\mathbf{T_{fR0}}\}$ is the zero frame of the mated conventional robot; $\{\mathbf{T_{S0}}\}$ is the zero frame of the shadow system; $\{\mathbf{T_D}\}$ is the desired target frame; $\{\mathbf{T_T}\}$ is the actual end-effecter frame; $\{\mathbf{T_{fRi}}\}$ is the joint frame of the robot, and $i = 1, 2, \ldots, 6$; and $\{\mathbf{T_{Sj}}\}$ is the joint frame of the shadow system, and $j = 1, 2, \ldots, 6$. In Fig. 4, the transformation from

https://doi.org/10.1017/S0263574704001171 Published online by Cambridge University Press

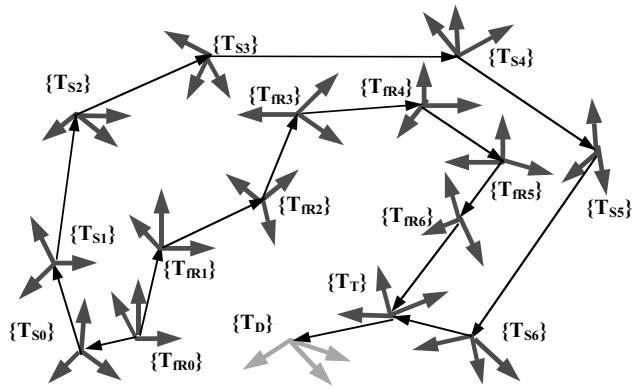


Fig. 4. Frame Transformation of the Ultra-precision Integrated Robotic System.

$\{\mathbf{T_{fR0}}\}$ to $\{\mathbf{T_{S0}}\}$ is ${}^{R0}_{S0}\mathbf{T}$, the transformation from $\{\mathbf{T_{S6}}\}$ to $\{\mathbf{T_T}\}$ is ${}^{6}_{T}\mathbf{T_S}$, and the transformation from $\{\mathbf{T_{fR6}}\}$ to $\{\mathbf{T_T}\}$ is ${}^{6}_{T}\mathbf{T_R}$. These transformation forms are determined in association with the design and manufacturing and all are known. The link transformation of the robot can be expressed as

$$ {}^{0}_{6}\mathbf{T_{fR}} = {}^{0}_{1}\mathbf{T_{fR}}\,{}^{1}_{2}\mathbf{T_{fR}}\,{}^{2}_{3}\mathbf{T_{fR}}\,{}^{3}_{4}\mathbf{T_{fR}}\,{}^{4}_{5}\mathbf{T_{fR}}\,{}^{5}_{6}\mathbf{T_{fR}} \tag{5} $$

$$ {}^{0}_{T}\mathbf{T_{fR}} = {}^{0}_{6}\mathbf{T_{fR}}\,{}^{6}_{T}\mathbf{T_{fR}} \tag{6} $$

Because of the errors of the robot, ${}^{0}_{6}\mathbf{T_{fR}}$ it is unknown, and so is ${}^{0}_{T}\mathbf{T_{fR}}$.

To resolve the inverse kinematics, a virtual 6 DOF robot is imaged to implement the same kinematic control process. The virtual robot is used with the same way as the real industrial robot; however, there are no any errors since it is ideal. The transformation of the ideal virtual robot is

$$ {}^{0}_{6}\mathbf{T_R} = {}^{0}_{1}\mathbf{T_R}\,{}^{1}_{2}\mathbf{T_R}\,{}^{2}_{3}\mathbf{T_R}\,{}^{3}_{4}\mathbf{T_R}\,{}^{4}_{5}\mathbf{T_R}\,{}^{5}_{6}\mathbf{T_R} \tag{7} $$

$$ {}^{0}_{T}\mathbf{T_R} = {}^{0}_{6}\mathbf{T_R}\,{}^{6}_{T}\mathbf{T_R} \tag{8} $$

It leads to

$$ {}^{0}_{T}\mathbf{T_R} = \mathbf{T_D} \tag{9} $$

$$ {}^{0}_{6}\mathbf{T_R} = {}^{0}_{T}\mathbf{T_R}\,{}^{6}_{T}\mathbf{T}^{-1}_{\mathbf{R}} = \mathbf{T_D}\,{}^{6}_{T}\,\mathbf{T}^{-1}_{\mathbf{R}} \tag{10} $$

With the robotic inverse kinematics analysis, the angular configurations of the virtual ideal rigid robot can be obtained, and

$$ \theta_{\mathrm{V}} = \{\theta_{1\mathrm{V}},\ \theta_{2\mathrm{V}},\ \theta_{3\mathrm{V}},\ \theta_{4\mathrm{V}},\ \theta_{5\mathrm{V}},\ \theta_{6\mathrm{V}}\}^{\mathrm{T}} \tag{11} $$

which is the absolute angular displacement with reference of the zero frame of the joint to control the integrated industrial robot. By using θ_{V} as the input of the joints of the robot, if the robot has no error, then

$$ {}^{0}_{T}\mathbf{T_{fR}} = {}^{0}_{T}\mathbf{T_R} = \mathbf{T_D} \tag{12} $$

However, because of errors, it leads

$$ {}^{0}_{T}\mathbf{T_{fR}} \neq {}^{0}_{T}\mathbf{T_R} \tag{13} $$

At this moment, if there is no effective way to resolve the problem, the robot will lose control since it cannot exactly determine its end-effecter frame. With the help of the shadow system, the end-effecter frame of robot in the space of the shadow system can be monitored. The exact end-effecter $\mathbf{T_T}$ within the space of the shadow system is ${}^{0}_{T}\mathbf{T_S}$

$$ {}^{0}_{T}\mathbf{T_S} = {}^{0}_{1}\mathbf{T_S}\,{}^{1}_{2}\mathbf{T_S}\,{}^{2}_{3}\mathbf{T_S}\,{}^{3}_{4}\mathbf{T_S}\,{}^{4}_{5}\mathbf{T_S}\,{}^{5}_{6}\mathbf{T_S}\,{}^{6}_{T}\mathbf{T_S} \tag{14} $$

and which is known based on the measurement of the shadow system. The transformation of $\mathbf{T_T}$ in the space of the robot is ${}^{0}_{T}\mathbf{T_{fR}}$, and it cannot be directly known. However, it can be obtained with the following transformation, and

$$ {}^{0}_{T}\mathbf{T_{fR}} = {}^{R0}_{S0}\mathbf{T}\,{}^{0}_{T}\mathbf{T_S} = {}^{0}_{6}\mathbf{T_{fR}}\,{}^{6}_{T}\mathbf{T_{fR}} \tag{15} $$

It leads to the determination of ${}^{0}_{6}\mathbf{T_{fR}}$, and

$$ {}^{0}_{6}\mathbf{T_{fR}} = {}^{0}_{T}\mathbf{T_{fR}}\,{}^{6}_{T}\mathbf{T}^{-1}_{\mathbf{fR}} = {}^{R0}_{S0}\mathbf{T}\,{}^{0}_{T}\mathbf{T_S}\,{}^{6}_{T}\mathbf{T}^{-1}_{\mathbf{fR}} \tag{16} $$

By driving the end-effecter of virtual robot to the current misplaced end-effecter of the robot, the solution of inverse kinematics is

$$ \theta_{\mathrm{f}} = \{\theta_{1\mathrm{f}}, \theta_{2\mathrm{f}}, \theta_{3\mathrm{f}}, \theta_{4\mathrm{f}}, \theta_{5\mathrm{f}}, \theta_{6\mathrm{f}}\}^{\mathrm{T}} \tag{17} $$

It is the actual angular displacements of the virtual robot. The difference caused by the errors is

$$ \begin{aligned} \theta_{\mathrm{V}} - \theta_{\mathrm{f}} = \{&\theta_{1\mathrm{V}} - \theta_{1\mathrm{f}}, \theta_{2\mathrm{V}} - \theta_{2\mathrm{f}}, \theta_{3\mathrm{V}} - \theta_{3\mathrm{f}}, \\ &\theta_{4\mathrm{V}} - \theta_{4\mathrm{f}}, \theta_{5\mathrm{V}} - \theta_{5\mathrm{f}}, \theta_{6\mathrm{V}} - \theta_{6\mathrm{f}}\}^{\mathrm{T}} \end{aligned} \tag{18} $$

that is,

$$ \delta\theta = \theta_{\mathrm{V}} - \theta_{\mathrm{f}} = \{\delta\theta_1, \delta\theta_2, \delta\theta_3, \delta\theta_4, \delta\theta_5, \delta\theta_6\}^{\mathrm{T}} \tag{19} $$

$\delta\theta$ is the feedback data needed for the mated industrial robot of the ultra-precision integrated robotic system to achieve the desired target in the next step. To cover the difference and to achieve the desired position and orientation of target, the joint configurations of inverse kinematics should have an extra displacement $\delta\theta$. The total absolute joint displacement referring to zero position with the mated robot is of the θ_{VT}, and

$$ \theta_{\mathrm{VT}} = \theta_{\mathrm{V}} + \delta\theta \tag{20} $$

If the end-effecter frame measured with the shadow system has still not reached the desired target frame, then, the next step yielding above process is needed. With the scheme of approach control step by step, the mated robot can finally achieve the desired target frame with ultra-precision kinematic accuracy. To implement the scheme of approach control, the joint actuating resolution of the integrated robot is required to match the joint measurement resolution of the shadow system. The requirement is considered lenient since the encoders used in shadow system are common components on current market.

Here, it is noted that, to conduct the above analysis of inverse kinematics, the integrated robotic system must have

https://doi.org/10.1017/S0263574704001171 Published online by Cambridge University Press

no interference between the shadow system and the industrial robot. To avoid such problems, the following necessary conditions can be further described as: If the working domain of heavy robot is H and the working domain of shadow robot is L, then, the necessary working condition of the integrated robot is $L \supseteq H$, and in the domain $L \cap H$, any elements of the two must not interfere each other. Obviously, with proper design, the problem of interferences can be avoided yielding above emphasized necessary conditions of the integrated robotic system design. Also, in future development, the singularities of the system are required to be further identified. Generally, if the singularity domain of heavy robot is A and the singularity domain of shadow robot is B, then, the singularity of the integrated robotic system is $AB = A \cup B$. Since the singularity domain of the integrated system is insignificant as compared with the entire working domain of the integrated robotic system, it will not influence the normal work of the system in general.

II.4. Error analysis

Since the nearly ideal shadow system is still not perfectly ideal, it is necessary to implement the error analysis to know the performance of the shadow system in application. The error analysis is particularly important to address the feasibility of the proposed technology. With a working process of the ultra-precision integrated robotic system, the target position of the end-effecter of the system can be written with a functional expression of

$$\mathbf{Y} = \mathbf{F}(\boldsymbol{\Theta}, \boldsymbol{\Phi}) \tag{21}$$

Here, $\boldsymbol{\Theta}$ is the system input set, which is defined in $\{\theta_1, \theta_2, \ldots, \theta_n\}$, the n-joint space of the shadow system. $\boldsymbol{\Phi}$ is the system construction set, which is defined in $\{\phi_1, \phi_2, \ldots, \phi_m\}$, the m-dimensional D-H parameter space associated with Denavit-Hartenberg (D-H) notation that are used to identify the shadow system.[19,20] With Taylor-series, the functional expression of the target can be further expressed as

$$\begin{aligned}\mathbf{Y} = \mathbf{F}(\boldsymbol{\Theta}^{\text{nom}}, \boldsymbol{\Phi}^{\text{nom}}) &+ \sum_{i=1}^{m} \frac{\partial \mathbf{F}}{\partial \phi_i}\bigg|_{\text{nom}} \left(\phi_i - \phi_i^{\text{nom}}\right) \\ &+ \sum_{j=1}^{n} \frac{\partial \mathbf{F}}{\partial \theta_i}\bigg|_{\text{nom}} \left(\theta_j - \theta_j^{\text{nom}}\right) + \frac{1}{2!}\left[\sum_{i=1}^{m} \frac{\partial^2 \mathbf{F}}{\partial \phi_i^2}\bigg|_{\text{nom}} \right. \\ &\left. \times \left(\phi_i - \phi_i^{\text{nom}}\right)^2 \sum_{j=1}^{n} \frac{\partial^2 \mathbf{F}}{\partial \theta_i^2}\bigg|_{\text{nom}} \left(\theta_j - \theta_j^{\text{nom}}\right)^2\right] + \cdots \end{aligned} \tag{22}$$

Here, $\boldsymbol{\Theta}^{\text{nom}} = \{\theta_1^{\text{nom}}, \theta_2^{\text{nom}}, \ldots, \theta_n^{\text{nom}}\}$ are the nominal joint displacements of the shadow system. $\boldsymbol{\Phi}^{\text{nom}} = \{\phi_1^{\text{nom}}, \phi_2^{\text{nom}}, \ldots, \phi_m^{\text{nom}}\}$ are the nominal D-H parameters of the shadow system. For small and independent variations, a linear approach of the Taylor series can be written as:[21,22]

$$\begin{aligned}\mathbf{Y} = \mathbf{F}(\boldsymbol{\Theta}^{\text{nom}}, \boldsymbol{\Phi}^{\text{nom}}) &+ \frac{\partial \mathbf{F}}{\partial \boldsymbol{\Phi}}\bigg|_{\text{nom}} (\boldsymbol{\Phi} - \boldsymbol{\Phi}^{\text{nom}}) \\ &+ \frac{\partial \mathbf{F}}{\partial \boldsymbol{\Theta}}\bigg|_{\text{nom}} (\boldsymbol{\Theta} - \boldsymbol{\Theta}^{\text{nom}}) \end{aligned} \tag{23}$$

It leads to the approximation equation

$$\Delta \mathbf{Y} = \frac{\partial \mathbf{F}}{\partial \boldsymbol{\Phi}} \Delta \boldsymbol{\Phi} + \frac{\partial \mathbf{F}}{\partial \boldsymbol{\Theta}} \Delta \boldsymbol{\Theta} \tag{24}$$

This is the analytic model of error of the shadow system. It relates component variability $\Delta\boldsymbol{\Phi}$ in D-H parameter space and measured angular displacement variability $\Delta\boldsymbol{\Theta}$ in the joint space of the shadow system to output error variation $\Delta\mathbf{Y}$ in Cartesian space, in which, all higher order effects are neglected.

III. EXAMPLE OF ERROR ANALYSIS WITH A PUMA 560 SHADOW SYSTEM

The following error analysis tries to theoretically demonstrate if the feasibility of the research can be verified with a practical example. In the embodiment of the shadow system, the basic construction of a 6 DOF Puma 560 robot is adopted except that all the actuators of Puma 560 are replaced with optical rotary encoders (Fig. 5). The reason to choose a Puma 560 is that all its joints are revolute. It is considered that a revolute joint is relatively easy to be manufactured with ultra-precision accuracy. In this case, since the shadow system stands only insignificant force, a set of zero clearance ultra-precision bearings mating with optical encoders can be adopted to build the joints. The dimensions of D-H parameters of the shadow system are $a_2 = 1\,\text{m}$, $a_3 = 0.02\,\text{m}$, $a_6 = 0.1\,\text{m}$, $d_1 = 1\,\text{m}$, $d_3 = 0.15\,\text{m}$, $d_4 = 0.6\,\text{m}$.

III.1. Derivation of the general analytic kinematic error of the system

Although the previous error estimation with extreme case gives the basic idea about the limitation of the kinematic accuracy, the general analysis of kinematic error of the system is also needed. In each of the steps associated with the approaching process, the general analytic kinematic error has to be used to justify the solution of the inverse kinematics for the end-effecter to finally reach the desired position and orientation of target. The processes of analytic error analysis are demonstrated below.

III.1.1. System mathematical model. The generalized mathematical model of shadow system corresponding to the position and orientation of target frame versus the angular displacements and D-H parameters is

$$\mathbf{Y} = \mathbf{F}(\boldsymbol{\Theta}, \boldsymbol{\Phi}) = \{P_X, P_Y, P_Z, \theta_R, \theta_P, \theta_Y\}^T \tag{25}$$

With the puma 560 shadow system, $\boldsymbol{\Theta}$ is defined in the joint space of $\{\theta_1, \theta_2, \theta_3, \theta_4, \theta_5, \theta_6\}$, $\boldsymbol{\Phi}$ is defined in D-H parameter space of $\{a_2, a_3, a_6, d_1, d_3, d_4\}$, and

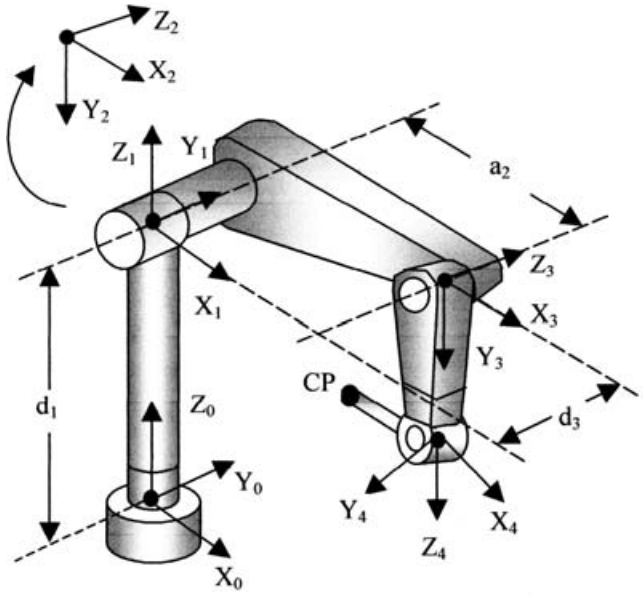
$$P_X = c_1(a_2c_2 + a_3c_{23} - d_4s_{23}) - d_3s_1 - r_{11}a_6 \tag{26}$$

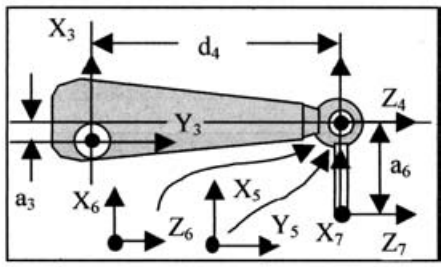
$$P_Y = s_1(a_2c_2 + a_3c_{23} - d_4s_{23}) + d_3c_1 - r_{21}a_6 \tag{27}$$

$$P_Z = -a_3s_{23} - a_2s_2 - d_4c_{23} + d_1 - r_{31}a_6 \tag{28}$$

$$\theta_R = \text{Atan2}(r_{32}, r_{33}) \tag{29}$$

https://doi.org/10.1017/S0263574704001171 Published online by Cambridge University Press





i	α_{i-1}	a_{i-1}	d_i	θ_i
1	0	0	d_1	θ_1
2	$-\pi/2$	0	0	θ_2
3	0	a_2	d_3	θ_3
4	$-\pi/2$	a_3	d_4	θ_4
5	$\pi/2$	0	0	θ_5
6	$-\pi/2$	0	0	θ_6
7	0	a_6	0	0

Link D-H parameters

Fig. 5. A Puma 560 Type Shadow System with CP Link.

$$\theta_P = \text{Atan2}\left(-r_{31}, \sqrt{r_{11}^2 + r_{21}^2}\right) \tag{30}$$

$$\theta_Y = \text{Atan2}(r_{21}, r_{11}) \tag{31}$$

Here,

$$c_i = \cos\theta_i, s_i = \sin\theta_i (i = 1, 2, \ldots, 6)$$

$$c_{23} = c_2c_3 - s_2s_3, s_{23} = c_2s_3 + s_2c_3$$

$$r_{11} = c_1[c_{23}(c_4c_5c_6 - s_4s_6) - s_{23}s_5c_6] + s_1(s_4c_5c_6 + c_4s_6)$$

$$r_{21} = s_1[c_{23}(c_4c_5c_6 - s_4s_6) - s_{23}s_5c_6] - c_1(s_4c_5c_6 + c_4s_6)$$

$$r_{31} = -s_{23}(c_4c_5c_6 - s_4s_6) - c_{23}s_5c_6$$

$$r_{12} = c_1[c_{23}(-c_4c_5s_6 - s_4c_6) + s_{23}s_5s_6] + s_1(c_4c_6 - s_4c_5s_6)$$

$$r_{22} = s_1[c_{23}(-c_4c_5s_6 - s_4c_6) + s_{23}s_5s_6] - c_1(c_4c_6 - s_4c_5s_6)$$

$$r_{32} = -s_{23}(-c_4c_5s_6 - s_4c_6) + c_{23}s_5s_6$$

$$r_{13} = -c_1(c_{23}c_4s_5 + s_{23}c_5) - s_1s_4s_5$$

$$r_{23} = -s_1(c_{23}c_4s_5 + s_{23}c_5) + c_1s_4s_5$$

$$r_{33} = s_{23}c_4s_5 - c_{23}c_5$$

III.1.2. System error analysis model. The analytical model of error corresponding to the puma 560 shadow system can then be obtained and written in the following form:

$$\Delta\mathbf{Y} = \frac{\partial\mathbf{F}}{\partial\mathbf{\Phi}}\Delta\mathbf{\Phi} + \frac{\partial\mathbf{F}}{\partial\mathbf{\Theta}}\Delta\mathbf{\Theta}$$

That is,

$$\begin{pmatrix}\Delta P_X\\ \Delta P_Y\\ \Delta P_Z\\ \Delta\theta_R\\ \Delta\theta_P\\ \Delta\theta_Y\end{pmatrix} = \begin{pmatrix}P_X\\ P_Y\\ P_Z\\ \theta_R\\ \theta_P\\ \theta_Y\end{pmatrix} \partial/\partial(\theta_1\theta_2\theta_3\theta_4\theta_5\theta_6 a_2a_3a_6d_1d_3d_4)_{nom}$$

$$\times (\Delta\theta_1\Delta\theta_2\Delta\theta_3\Delta\theta_4\Delta\theta_5\Delta\theta_6\Delta a_2\Delta a_3\Delta a_6\Delta d_1\Delta d_3\Delta d_4)^T \tag{32}$$

Here, $\Delta\theta_1$, $\Delta\theta_2$, $\Delta\theta_3$, $\Delta\theta_4$, $\Delta\theta_5$, and $\Delta\theta_6$ are the measurement errors of joint angular displacement of the shadow system, and Δa_2, Δa_3, Δa_6, Δd_1, Δd_3, and Δd_4 are the measurement errors of D-H structural parameter of the shadow system. The position and orientation errors of the end-effecter frame can then be determined below:

$$ERR = \pm\left\{\left(\Delta P_X^2 + \Delta P_Y^2 + \Delta P_Z^2\right)^{1/2}, (\Delta\theta_R, \Delta\theta_P, \Delta\theta_Y)\right\} \tag{33}$$

III.2. Determination of the ranges of measured kinematic errors

To determine the range of measured kinematic error, the following simulation is designed with the change of each of joints of the shadow system in turn. With the arrangements of the simulation, the common with 4,608,000 resolution rotary encoder and the ultra-precision 32-bit resolution rotary encoder are employed for the theoretic discussions of the development. By using the above analytic kinematic error model, the kinematic error can be determined with nominal joint displacements, joint angular measurement errors, and

https://doi.org/10.1017/S0263574704001171 Published online by Cambridge University Press

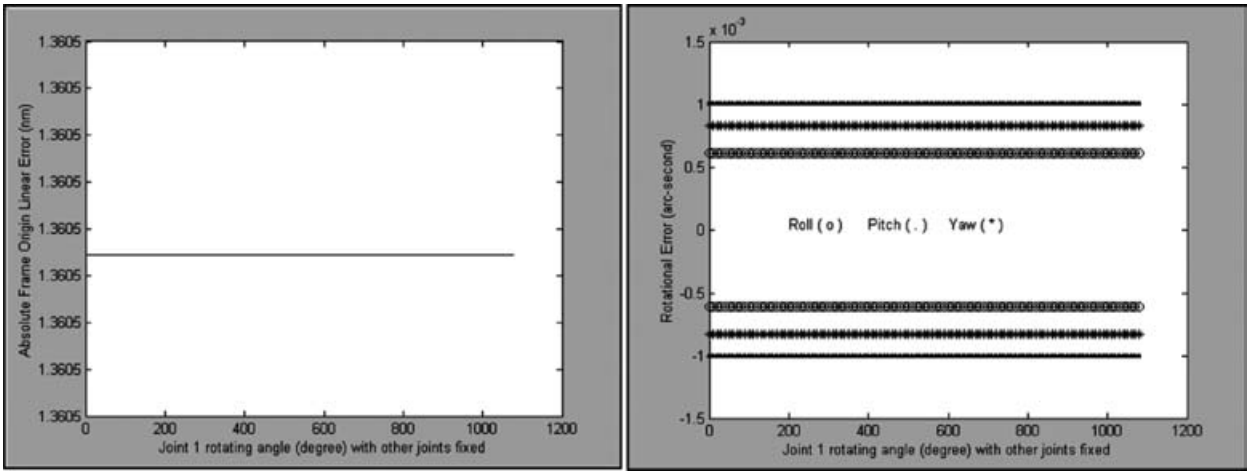


Fig. 6. Analytical Errors with Joint 1 Rotating and Other Joints Fixed (32-bit resolution) $\theta = \{\theta_1 = 0 \sim 1080;\ \theta_2 = 218;\ \theta_3 = 210;\ \theta_4 = 71;\ \theta_5 = 84;\ \theta_6 = 39\}$.

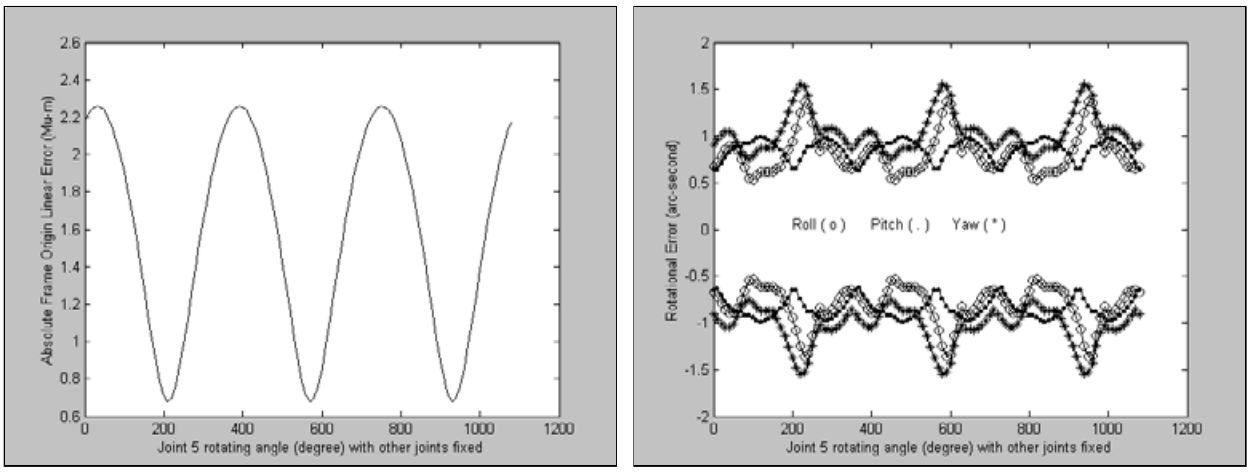


Fig. 7. Analytical Errors with Joint 2 Rotating and Other Joints Fixed (32-bit resolution) $\theta = \{\theta_1 = 67;\ \theta_2 = 0 \sim 1080;\ \theta_3 = 214;\ \theta_4 = 172;\ \theta_5 = 183;\ \theta_6 = 40\}$.

calibration errors of dimensional D-H parameter. In this case, the arrangements and values of the simulation are given below:

$$\begin{aligned}\boldsymbol{\Theta}|_{\text{nom}} &= \{\Delta\theta_1, \Delta\theta_2, \Delta\theta_3, \Delta\theta_4, \Delta\theta_5, \Delta\theta_6\}|_{\text{nom}} \\ &= \{\theta_{1\text{nom}}, \theta_{2\text{nom}}, \theta_{3\text{nom}}, \theta_{4\text{nom}}, \theta_{5\text{nom}}, \theta_{6\text{nom}}\} \\ \boldsymbol{\Phi}|_{\text{nom}} &= \{a_2, a_3, a_6, d_1, d_3, d_4\} \\ &= \{1, 0.02, 0.2, 1, 0.15, 0.6\}(\text{m})\end{aligned}$$

With embodiment of using 4,608,000 resolution rotary encoder:

$$\begin{aligned}\Delta\boldsymbol{\Theta} &= \{\Delta\theta_1, \Delta\theta_2, \Delta\theta_3, \Delta\theta_4, \Delta\theta_5, \Delta\theta_6\} \\ &= \pm\{0.28, 0.28, 0.28, 0.28, 0.28, 0.28\}(\text{arc-second}) \\ \Delta\boldsymbol{\Phi} &= \{\Delta a_2, \Delta a_3, \Delta a_6, \Delta d_1, \Delta d_3, \Delta d_4\} \\ &= \pm\{1, 1, 1, 1, 1, 1\}(\mu\text{m})\end{aligned}$$

With embodiment of using ultra-precision 32-bit resolution rotary encoder:

$$\begin{aligned}\Delta\boldsymbol{\Theta} &= \{\Delta\theta_1, \Delta\theta_2, \Delta\theta_3, \Delta\theta_4, \Delta\theta_5, \Delta\theta_6\} \\ &= \pm\{3, 3, 3, 3, 3, 3\}10^{-4}(\text{arc-second}) \\ \Delta\boldsymbol{\Phi} &= \{\Delta a_2, \Delta a_3, \Delta a_6, \Delta d_1, \Delta d_3, \Delta d_4\} \\ &= \pm\{1, 1, 1, 1, 1, 1\}(\text{nm})\end{aligned}$$

To determine the range of measured position and orientation errors with the change of each of the joints in turn, the algorithm of the simulation processes can be designed as follows:

1. Simulation input designation
   Let $\theta_{\text{inom}} = 0^\circ,\ 10^\circ,\ 20^\circ, \ldots, 1080^\circ$, and fix the other θ_j at a random position in the robot joint space; here, $i = (1, 2, 3, 4, 5, 6) \parallel j = (1, 2, 3, 4, 5, 6) \parallel j \neq i$
2. Obtain the simulated errors of the end-effecter frame $\text{ERR} = \pm\{(\Delta P_X^2 + \Delta P_Y^2 + \Delta P_Z^2)^{1/2}, (\Delta\theta_R, \Delta\theta_P, \Delta\theta_Y)\}$
3. Draw curves of the simulated errors versus change of θ_{inom} with fixed θ_j

https://doi.org/10.1017/S0263574704001171 Published online by Cambridge University Press

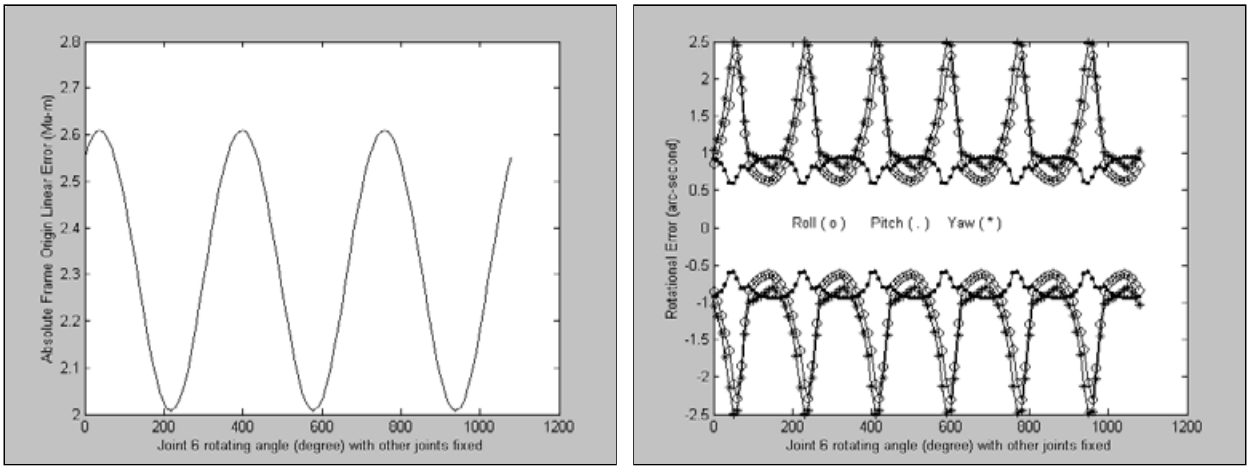


Fig. 8. Analytical Errors with Joint 3 Rotating and Other Joints Fixed (32-bit resolution) $\theta = \{\theta_1 = 88;\ \theta_2 = 18;\ \theta_3 = 0 \sim 1080;\ \theta_4 = 174;\ \theta_5 = 181;\ \theta_6 = 132\}$.

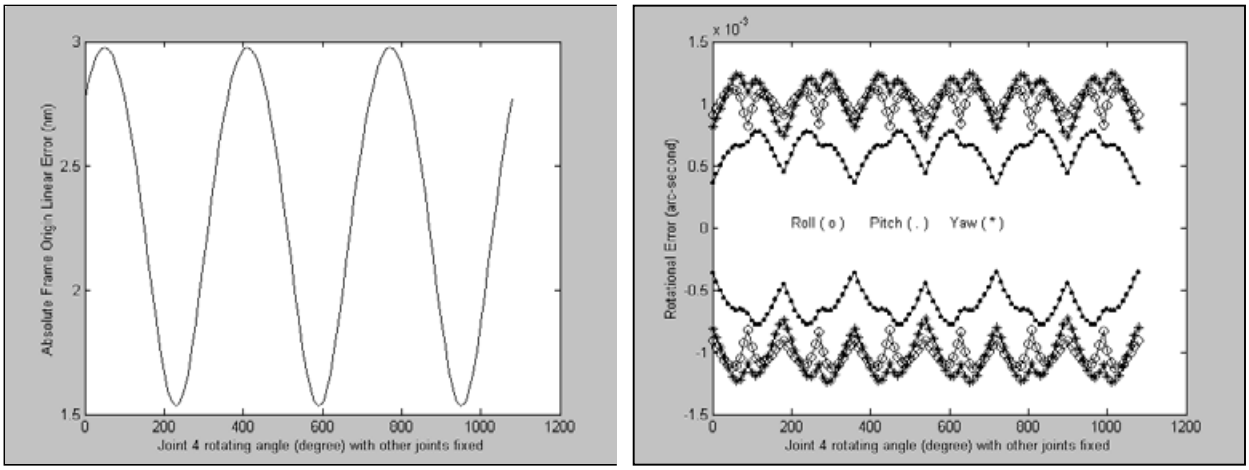


Fig. 9. Analytical Errors with Joint 4 Rotating and Other Joints Fixed (32-bit resolution) $\theta = \{\theta_1 = 186;\ \theta_2 = 118;\ \theta_3 = 22;\ \theta_4 = 0 \sim 1080;\ \theta_5 = 12;\ \theta_6 = 92\}$.

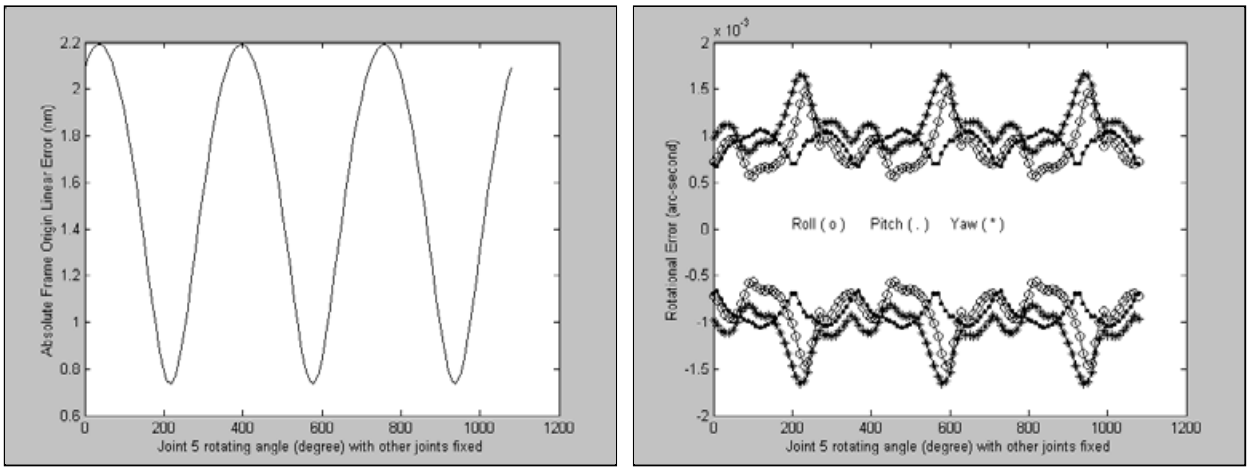


Fig. 10. Analytical Errors with Joint 5 Rotating and Other Joints Fixed (32-bit resolution) $\theta = \{\theta_1 = 86;\ \theta_2 = 318;\ \theta_3 = 92;\ \theta_4 = 73;\ \theta_5 = 0 \sim 1080;\ \theta_6 = 12\}$.

The corresponding simulation of kinematic accuracies and ranges with the shadow system are arrangement through two cases of the expectations of the research with random determination of nominal configurations. In the first case of simulation, the ultra-precision 32-bit resolution rotary encoder is used to build the shadow system, and the simulation results are depicted shown from Fig. 6 to Fig. 11. In the second case, the common 0.28 arc-second resolution

https://doi.org/10.1017/S0263574704001171 Published online by Cambridge University Press

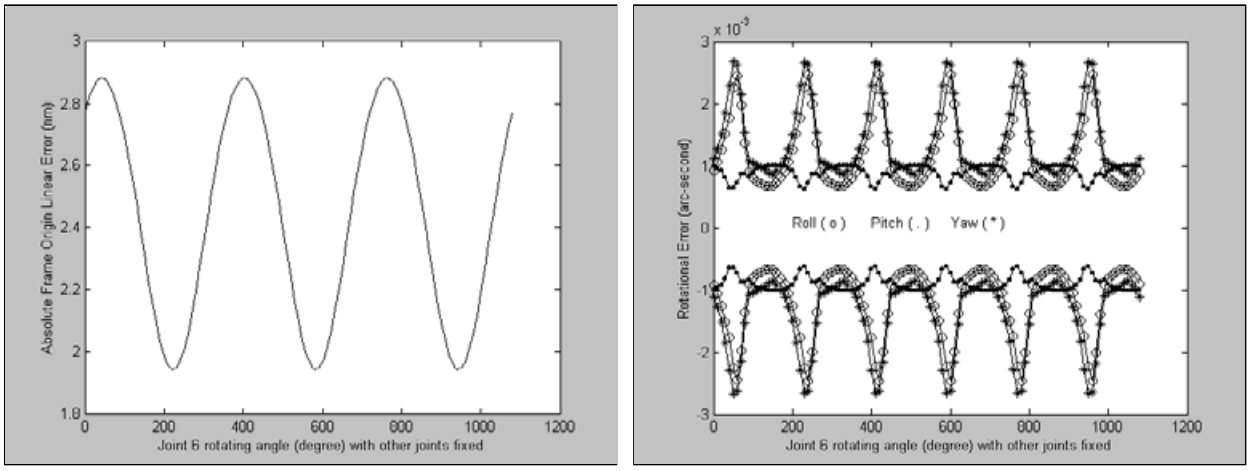


Fig. 11. Analytical Errors with Joint 6 Rotating and Other Joints Fixed (32-bit resolution) $\theta = \{\theta_1 = 217;\ \theta_2 = 38;\ \theta_3 = 193;\ \theta_4 = 91;\ \theta_5 = 232;\ \theta_6 = 0 \sim 1080\}$.

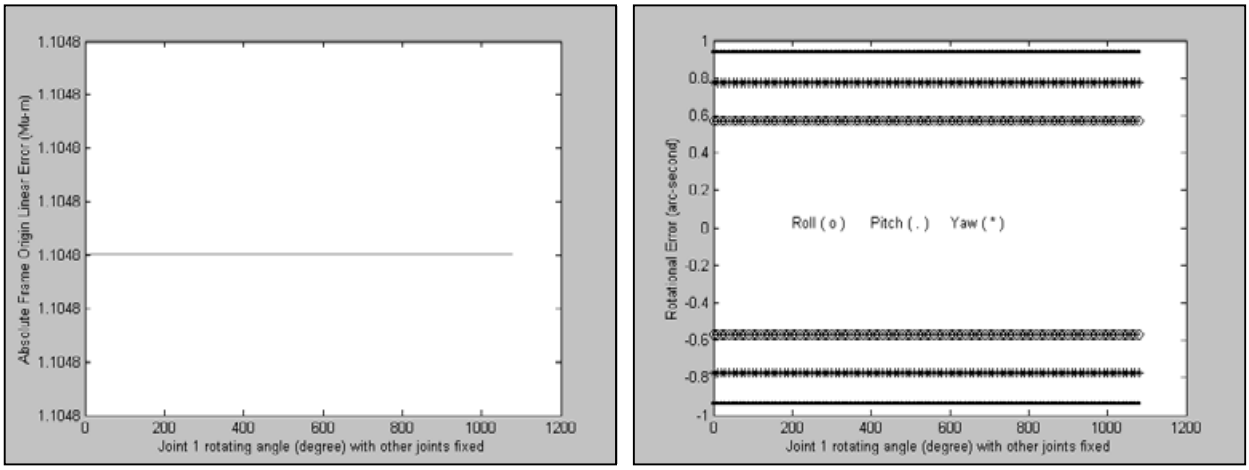


Fig. 12. Analytical Errors with Joint 1 Rotating and Other Joints Fixed (0.28 arc-second resolution) $\theta = \{\theta_1 = 0 \sim 1080;\ \theta_2 = 218;\ \theta_3 = 210;\ \theta_4 = 71;\ \theta_5 = 84;\ \theta_6 = 39\}$.

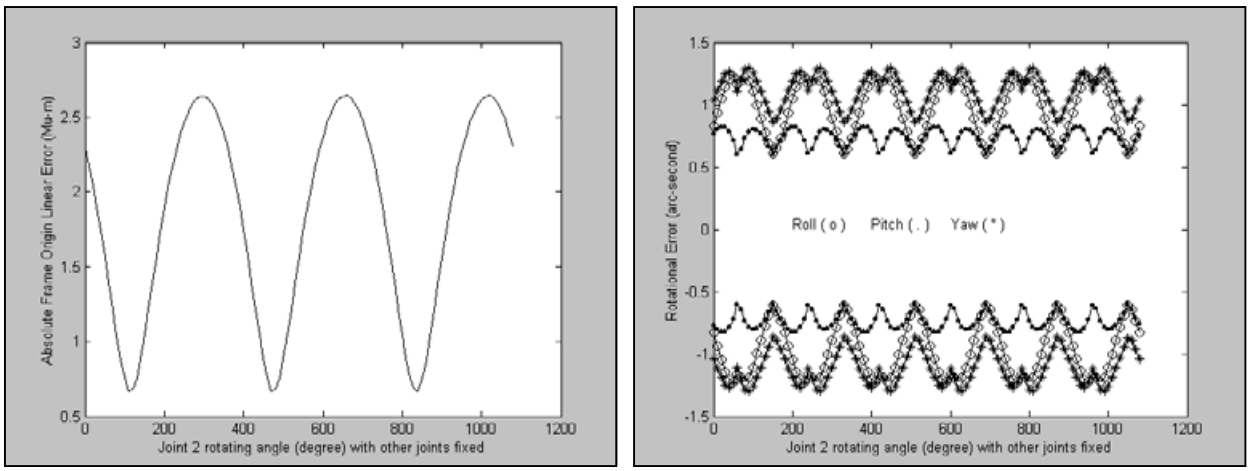


Fig. 13. Analytical Errors with Joint 2 Rotating and Other Joints Fixed (0.28 arc-second resolution) $\theta = \{\theta_1 = 67;\ \theta_2 = 0 \sim 1080;\ \theta_3 = 214;\ \theta_4 = 172;\ \theta_5 = 183;\ \theta_6 = 40\}$.

rotary encoder is adopted, and the simulation results are depicted from Fig. 12 to Fig. 17.

Through the simulation results from Fig. 6 to Fig. 17, it appears that, in the highly correlated Puma 560 joint and D-H spaces, the kinematic accuracy of the shadow system can still quite easy to achieve the rounded two goals. Although the implementation of the embodiment is conducted by the use of the existing rotary encoders on the current market, the results

https://doi.org/10.1017/S0263574704001171 Published online by Cambridge University Press

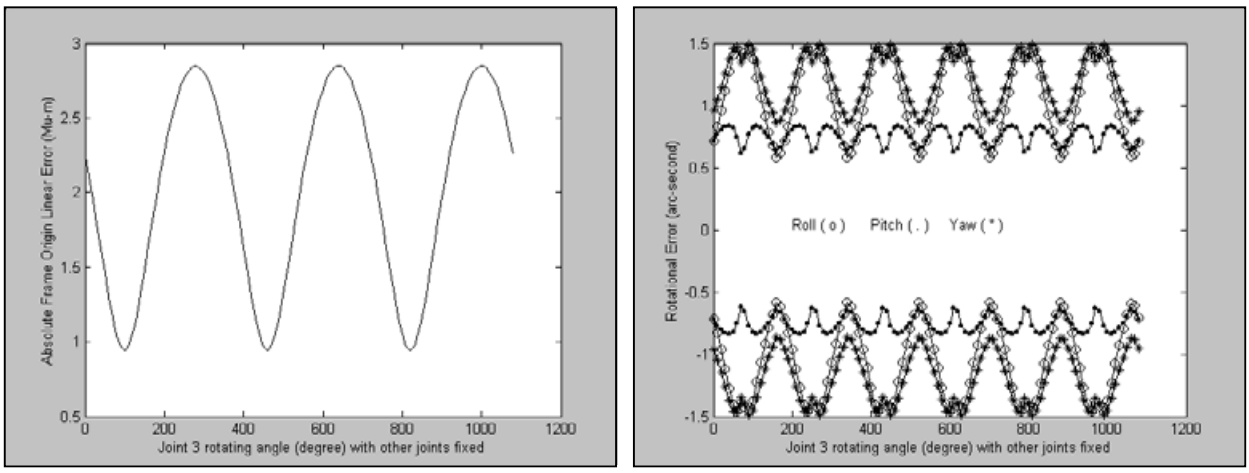


Fig. 14. Analytical Errors with Joint 3 Rotating and Other Joints Fixed (0.28 arc-second resolution) $\theta = \{\theta_1 = 88;\ \theta_2 = 18;\ \theta_3 = 0 \sim 1080;\ \theta_4 = 174;\ \theta_5 = 181;\ \theta_6 = 132\}$.

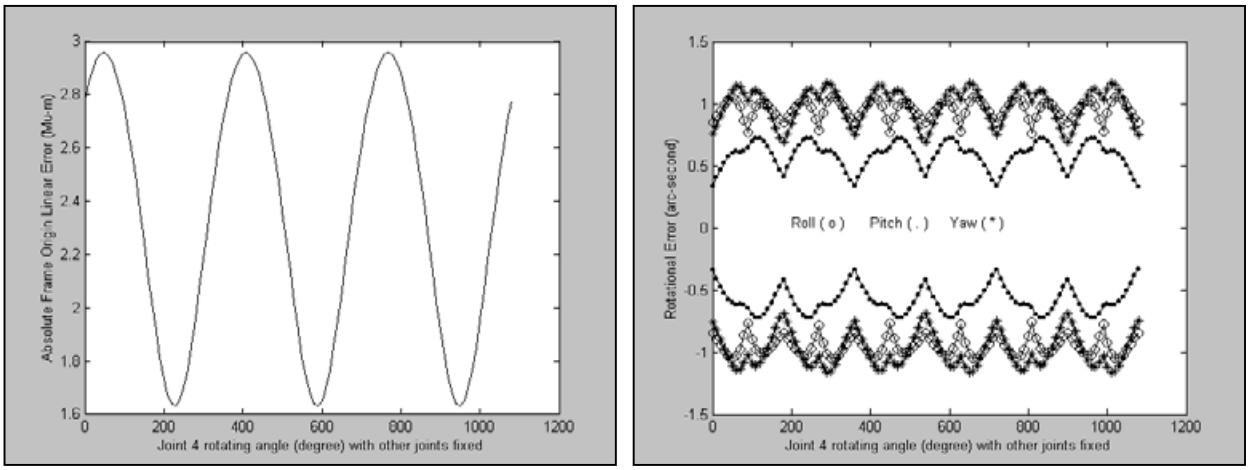


Fig. 15. Analytical Errors with Joint 4 Rotating and Other Joints Fixed (0.28 arc-second resolution) $\theta = \{\theta_1 = 186;\ \theta_2 = 118;\ \theta_3 = 22;\ \theta_4 = 0 \sim 1080;\ \theta_5 = 12;\ \theta_6 = 92\}$.

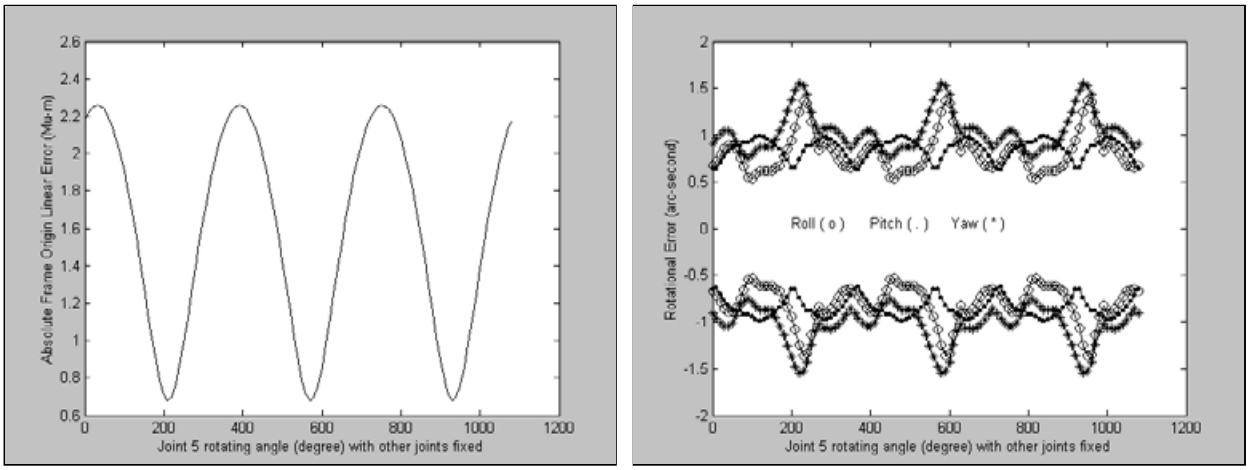


Fig. 16. Analytical Errors with Joint 5 Rotating and Other Joints Fixed (0.28 arc-second resolution) $\theta = \{\theta_1 = 86;\ \theta_2 = 318;\ \theta_3 = 92;\ \theta_4 = 73;\ \theta_5 = 0 \sim 1080;\ \theta_6 = 12\}$.

have already demonstrated the significant development of the kinematic accuracy. As above-discussed, to date, it is still struggle for a robotic system to achieve the kinematic accuracy in level of $\{0.025\,\text{mm},\ 5\ \text{arc-second}\}$. Therefore, the immediate impact of this research to the development of ultra-precision industrial robot is obvious.

https://doi.org/10.1017/S0263574704001171 Published online by Cambridge University Press

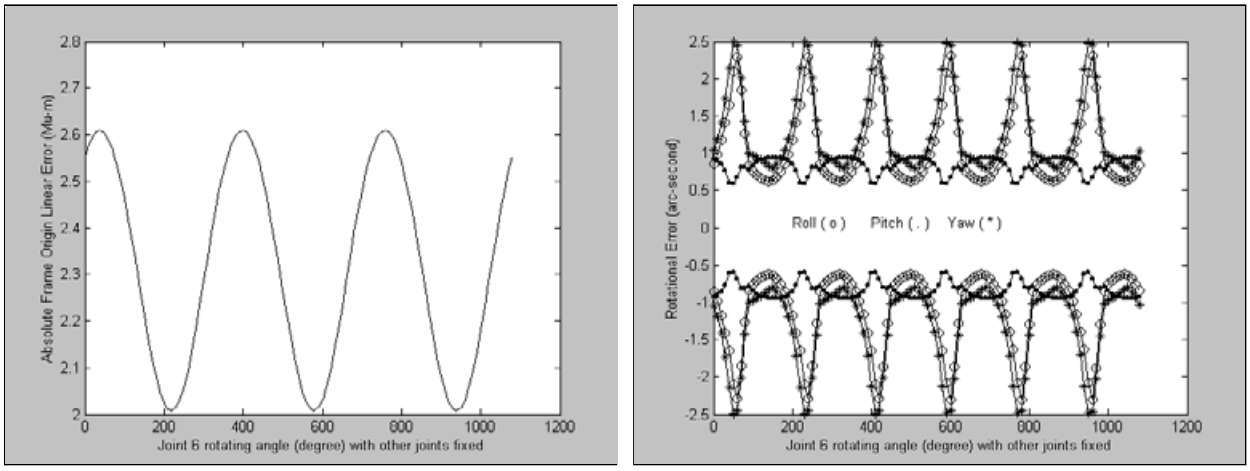


Fig. 17. Analytical Errors with Joint 6 Rotating and Other Joints Fixed (0.28 arc-second resolution) $\theta = \{\theta_1 = 217;\ \theta_2 = 38;\ \theta_3 = 193;\ \theta_4 = 91;\ \theta_5 = 232;\ \theta_6 = 0 \sim 1080\}$.

IV. CONCLUSIONS

The most meaningful portion of the research is that it presents a novel design methodology for the development of ultra-precision industrial robot. Such a different theoretical approach for a robot to achieve the ultra-precision kinematic accuracy conducts the enrichment of the design theories in robotics.

With the theoretic simulation of the development, it demonstrates that an integrated robotic system built with the 4,608,000 resolution and the ultra-precision 32-bit resolution rotary encoders on the market can achieve the kinematic accuracy up to {10 μm, 2.5 arc-second} and {10 nm, 10^{-2} arc-second} respectively. Obviously, the technology is suitable not only for the rigid body robot but also for the RYLDA. This is considered as the most significant aspect of the research since it conducts an immediate impact to the development of ultra-precision industrial robot in general. It is known that, currently, the RYLDA is still considered somewhat difficult to have "under-control" status, and the kinematic accuracy of RYLDA is still relatively rough. In such a circumstance, the research could play a role to accelerate the development of ultra-precision RYLDA technology.

It is noted that to pursue the precision control of a robotic system in the scope of nano-meter kinematic accuracy is an exceptional level of performance, and there is still a long way to go from the current level to the final realization of the ultra-precision integrated robotic system in industrial practice and academic research. However, the result with this research has gained the very most important and necessary first step with its way for the development of ultra-precision industrial robot in general.

References

1. *Thomas Register of American Manufacturers* (Thomas Publishing Company, 2002).
2. S. Tzafestas, "Guest editorial: Flexible-joint and flexible-link robots," *Journal of Intelligent and Robotic Systems: Theory and Applications* **34**(4), 331–333 (2002).
3. G. LeVey et al., "Flexible links manipulators: From modelling to control," *Journal of Intelligent and Robotic Systems: Theory and Applications* **34**(4), 381–414 (2002).
4. M. Shaheed and M. Tokhi, "Dynamic modelling of a single-link flexible manipulator: Parametric and non-parametric approaches," *Robotica* **20**(1), 93–109 (2002).
5. J. Martins, Jorge, M. Ayala Botto and J. Da Costa, "Modeling of flexible beams for robotic manipulators," *Multibody System Dynamics* **7**(1), 79–100 (2002).
6. W. Xu et al., "Point-to-point trajectory planning of flexible redundant robot manipulators using genetic algorithms," *Robotica* **20**(3), 269–280 (2002).
7. M. Yamano et al., "Cooperative control of a 3D dual-flexible-arm robot," *Journal of Intelligent and Robotic Systems: Theory and Applications* **39**(1), 1–15 (2004).
8. H. Christensen and P. Corke, "Editorial: Special issue on visual servoing," *International Journal of Robotics Research* **22**(10–11), 779–780 (2003).
9. P. Jiang and R. Unbehauen, "Robot visual servoing with iterative learning control," *IEEE Transactions on Systems, Man, and Cybernetics Part A: Systems and Humans* **32**(2), 281–287 (2002).
10. T. Hamel and R. Mahony, "Visual servoing of an under-actuated dynamic rigid-body system: An image-based approach," *IEEE Transactions on Robotics and Automation* **18**(2), 187–198 (2002).
11. K. Hashimoto, "A review on vision-based control of robot manipulators," *Advanced Robotics* **17**(10), 969–991 (2003).
12. D. Kragic and H. Christensen, "Robust visual servoing," *International Journal of Robotics Research* **22**(10–11), 923–939 (2003).
13. J. Zhang and C. Meng, "A linear/angular interferometer capable of measuring large angular motion," *Journal of Measurement Science and Technology* **10**, 1247–1253 (1999).
14. O. Cíp and F. Petru, "A scale-linearization method for precise laser interferometry," *Journal of Measurement Science and Technology* **11**, 133–141 (2000).
15. S. Gong, "A novel conceptual ultra-precision dimensional measurement technology," *Journal of Measurement* **33**(I4), 347–357 (2003).
16. S. Tao et al., "Vibration control for a flexible-link robot arm with deflection feedback," *International Journal of Non-Linear Mechanics* **38**(1), 51–62 (2003).
17. Z. Mohamed and M. Tokhi, "Command shaping techniques for vibration control of a flexible robot manipulator," *Mechatronics* **14**(1), 69–90 (2004).

https://doi.org/10.1017/S0263574704001171 Published online by Cambridge University Press

18. D. Sun et al., "A PZT actuator control of a single-link flexible manipulator based on linear velocity feedback and actuator placement," *Mechatronics* **14**(4), 381–401 (2004).
19. J. Denavit and R. Hartenberg, "A kinematic Notation for low-pair mechanisms based on matrixes," *Journal of Applied Mechanics* 215–221 (1955).
20. J. Craig, *Introduction to Robotics* (Addison-Wesley Publishing Company, 1986).
21. I. Sneddon (ed.), Encyclopaedic Dictionary of Mathematics for Engineers and Applied Scientists (Pergamon Press, 1976).
22. J. Chakraborty, "Synthesis of mechanical error in linkages," *Journal of Mechanism and Machine Theory* **10**, 155–165 (1975).

https://doi.org/10.1017/S0263574704001171 Published online by Cambridge University Press